Unusual enhancements of B_{c2} and T_c in the restacked TaS_2 nanosheets

Yonghui Ma[1,3,4], Jie Pan[2,4], Chenguang Guo[2,4], Xuan Zhang[1], Lingling Wang[1], Tao Hu[1,3], Gang Mu[1,3,*], Fuqiang Huang[2,3,†], and Xiaoming Xie[1,3]

Recently we reported an enhanced superconductivity in restacked monolayer TaS_2 nanosheets compared with the bulk TaS_2, pointing to the exotic physical properties of low dimensional systems. Here we tune the superconducting properties of this system with magnetic field along different directions, where a strong Pauli paramagnetic spin-splitting effects is found in this system. Importantly, an unusual enhancement as high as 3.8 times of the upper critical field B_{c2} is observed under the inclined external magnetic field. Moreover, with the vertical field fixed, we find that the superconducting transition temperature T_c can be enhanced by increasing the transverse field and forms a dome-shaped phase diagram. We argue that the restacked crystal structure without inversion center along with the strong spin-orbit coupling may paly a key role for our observations. The present findings are significant in the viewpoint of fundamental physics and may also facilitate the applications of low-dimensional superconductors in the environment of high field.

[1]State Key Laboratory of Functional Materials for Informatics, Shanghai Institute of Microsystem and Information Technology, Chinese Academy of Sciences, Shanghai 200050, China. [2]State Key Laboratory of High Performance Ceramics and Superfine Microstructure, Shanghai Institute of Ceramics, Chinese Academy of Sciences, Shanghai, 200050, China. [3]CAS Center for Excellence in Superconducting Electronics (CENSE), Shanghai 200050, China. [4]University of Chinese Academy of Sciences, Beijing 100049, China. Correspondence and requests for materials should be addressed to G.M. (email: mugang@mail.sim.ac.cn) and F.Q.H. (email: huangfq@mail.sic.ac.cn). Y.H.M. and J.P contributed equally to this work.

Superconductivity in low-dimensional systems was investigated extensively recently, due to the fertile physical phenomenon and exotic properties [1–5]. At present, the gate of this research field has just been opened and more interesting phenomena are waiting to be explored. Magnetic field is one of the fundamental tuning parameters to affect the behaviors of a superconductor. In the type-II superconductors, the magnetic field can penetrate into the bulk in the form of quantized vortex lines when it exceeds the lower critical field B_{c1} [6]. Because of the strong spin-orbit coupling, superconducting transition metal dichalcogenides (TMDs) are investigated intensively in the two-dimensional limit in recent years [7–10], where a clear enhancement of the in-plane upper critical field are frequently reported, which were interpreted by the Zeeman-protected Ising superconductivity mechanism. Using a chemical exfoliation method, we have obtained the monolayer TaS_2 nanosheets, which were assembled layer-by-layer by vacuum filtration [11,12]. Such a restacked material shows superconductivity with T_c ($\sim$ 3.2 K) several times higher than the pristine bulk 2H-TaS_2, which supplies a significant platform for studying the intrinsic physical properties of unconventional superconductors in TMDs. However, the in-depth investigation on the physical behaviors of this material is lacking and more experiments are required at present.

Here we present a detailed investigation on the Abrikosov vortex phase of the above-mentioned superconductor, restacked TaS_2 nanosheets, by measuring the conducting properties with magnetic fields along different directions. The upper critical field within the ab-plane B_{c2}^{ab} is clear larger than the Pauli paramagnetic limiting fields B_P, indicating a strong Pauli paramagnetic spin-splitting effects in this material. Importantly, the angular dependence of the upper critical field deviates severely from the Ginzburg-Landau (GL) model and Tinkham model. Moreover, the value of T_c

is found to increase with the transverse field $B_{\|ab}$ under a fixed vertical field $B_{\|c}$. We found that the highly noncentrosymmetric crystal structure and the strong spin-orbit coupling are key factors for the unusual behaviors we observed. Our results may promote the studies on the fundamental physics and applications in this field.

Results

Details regarding the samples preparation and resistance measurements are given in the Methods section. By a careful characterization using combining methods, the structure of the restacked TaS_2 was determined and reported in our previous paper [11]. The inter-layer spacing is close to bulk 2H-TaS_2, while the 2H symmetry has been broken after the restacking process because of rotations between different layers (see Figure S1). In such a structure, both the in-plane inversion symmetry in each individual layer and the global inversion symmetry are broken. As a consequent, the inversion symmetry breaking will be stronger than the bulk, monolayer, and few layered TaS_2 materials. Very recently, a detailed investigation on the thickness dependence of superconducting behaviors of 2H-TaS_2 was reported [13], supplying a good coordinate to make a comparison. It is found that the critical transition temperature T_c increases with the decrease of thickness and reaches 3.4 K for monolayer TaS_2. This value is very close to our sample, confirming the monolayer-features of our sample and suggesting that the restacking process imposed on the monolayer TaS_2 doesn't affect the T_c of this system. Moreover, the normal state resistivity displays a $T^{2.45}$ behavior in low temperature in our sample (see Figure S2), corresponding to the situation between 3-layer ($\sim T^2$) and 7-layer ($\sim T^3$) for the ordered stacked TaS_2 [13]. This implies that the inter-layer coupling in our samples shows a certain degree of influence on the electrical transport behavior.

The resistive transitions of one sample (denoted as #1) measured in magnetic fields for both $B \parallel ab$ and $B \parallel c$ are shown in Figure 1a and b. Clear different efficiencies for the suppression of superconductivity, revealing the anisotropy of the present material, can be seen by comparing the two figures. To determine the upper critical fields B_{c2}, a criterion of 90% of the normal state resistance (R_n) is used and the results are shown in the Figure 1c for the two orientations. Instead of the square root behavior for the in-plane upper critical field ($B_{c2}^{ab} \sim \sqrt{1 - T/T_c}$) expected for the 2D superconductors [7–10,13], an opposite tendency with the positive curvature is observed, which has been found to be a universal feature of anisotropic 3D layered superconductors [14,15]. Again, this reflects the influence of inter-layer coupling on the in-plane upper critical field of our samples, although such a inter-layer stacking manner doesn't affect T_c. The value of B_{c2} at zero temperature can be estimated using the Werthamer-Helfand-Hohenberg relation [16] $B_{c2} = -0.693 \times dB_{c2}(T)/dT|_{T_c} \times T_c$ after the slope $dB_{c2}(T)/dT|_{T_c}$ is obtained from Figure 1c. In addition, the paramagnetic limiting field B_P has a simple relation with T_c, $B_P = 1.84 \times T_c$ based on the conventional BCS theory [17]. The resultant values for the three characteristic field B_{c2}^{ab} (in-plane B_{c2}), B_{c2}^{c} (out-plane B_{c2}) and B_P are denoted by arrows in Figure 1c and summarized in Table 1, from which the anisotropy of upper critical field $\Gamma = B_{c2}^{ab}/B_{c2}^{c} = 11$ is obtained. This value is larger than most of the iron-based superconductors and the copper-based superconductor YBCO [15,18]. Moreover, a clear relative relation $B_{c2}^{c} < B_P < B_{c2}^{ab}$ can be deduced.

Field-angle resolved experiments are performed by measuring the field (B) and angle (θ)

dependence of resistance at a fixed temperature 2.2 K. As shown in Figure 2a, one can see how the resistance is triggered by the field from zero to finite values and saturates gradually at high fields. In order to determine the precise onset superconducting transition point, which reflects the information of upper critical fields B_{c2}, we show the first derivative dR/dB of four typical curves in Figure 2b. As indicated by the arrows, the onset transition point is defined by the characteristic field where the value of dR/dB begins to increase clearly. The characteristic points determined in Figure 2b are represented by arrows in Figure 2a, the connection of which forms a slightly inclined straight line as shown by the blue dashed line. Based on this line reflecting the normal states resistance R_n, a criterion of $90\%R_n$, as revealed by the black dashed line, is adopted to define the upper critical fields. The crossing points between this black dashed line and the data curves in Figure 2a determine the upper critical field at different angles $B_{c2}(\theta)$. Angular dependence of $B_{c2}(\theta)$ normalized by B_{c2}^c is shown in Figure 2c. One can see the detailed evolution of $B_{c2}(\theta)/B_{c2}^c$ versus θ. In order to quantitatively evaluate such an angular dependent variation tendency, we employ two theoretical models, the 3D GL model and 2D Tinkham model [19,20] (see the Supplementary Information), and plot them in this figure for comparison. These two models show slight differences near $\theta = 90^o$, which is usually used to distinguish the 2D superconductivity in monolayer or interfacial systems [8,9,21]. We note that such a discrimination process is found to be credible and valid in a high temperature near T_c. However, the difference between the experimental data and the two models is much larger, showing a great enhancement of upper critical field in the angle range $30^o < \theta < 85^o$ as revealed in the area with yellow shadow. In the strong anisotropic system, the perpendicular component of the the upper critical field $B_{c2}(\theta)cos\theta$ is expected to be dominant in the low angle range since the in-plane magnetic field is not important in terms of suppressing T_c. So we show this component normalized by B^c_{c2} in Figure 2d, where a broad peak-shaped experimental curve with the maximum enhancement of 3.8 times is observed.

Actually such an upper-critical-field-enhancement effect can induce very fascinating features in T_c in the mixed state. Here we adopt a different mode of measurements: $R-T$ curves are measured with the vertical field $B_{\|c}$ fixed and the transverse field $B_{\|ab}$ increasing, as schematized in Figure 3a. This method has been used to identify the 2D or interfacial superconductivity, where the curves will overlap with each other because $B_{\|ab}$ is not important in an extremely 2D superconductor [21,22]. While in a anisotropic system with 3D features, T_c will be reasonably suppressed by $B_{\|ab}$ (see the Supplementary Information). In Figure 3b we show a typical set of data with $B_{\|c} = 0.4$ T on another sample denoted as #2 with a similar T_c as #1. The behavior is uniquely different from the above-mentioned two categories. The superconducting transition is enhanced clearly following by a suppression with the increasing of $B_{\|ab}$. Three criterions, $10\%R_n$, $50\%R_n$, and $90\%R_n$, are employed to determine the critical transition temperature T_c and the results are shown in Figure 3c. All the three curves show the dome-like features, confirming that it is an intrinsic property rather than a magnetic flux-related behavior. The dome-like behavior may reveal the presence of competing between some unconventional effect and the pairing-breaking effect induce by magnetic field. Figure 3d summarizes a 3D phase diagram showing the effect of $B_{\|ab}$ on T_c at different $B_{\|c}$, where T_c is determined using the criterion $50\%R_n$.

Discussion

From the comparisons between our results and that reported by Y. Yang et al. [13], our samples of the restacked TaS_2 monolayers maintain the enhanced T_c (compared with the bulk material), while lose the 2D characters and show the anisotropic 3D features. A more careful examination shows that the out-plane upper critical field B_{c2}^{c} is similar to the bilayer TaS_2, while the in-plane B_{c2}^{ab} and the anisotropy are only one third of the bilayer TaS_2. Nevertheless, B_{c2}^{ab} of our samples is clearly larger than that of the bulk samples since the latter doesn't exceed the Pauli limit. All in all, the present samples are different from both the monolayered and the bulk TaS_2.

Intuitively, the theoretical proposal [23–25] predicting a field-induced triplet component in the order parameter of the singlet superconductors due to the Pauli paramagnetic spin-splitting effects is very consistent with our observation shown in Figure 2(d). According to their arguments, such an enhancement of $B_{c2}(\theta)$ should be conspicuous in anisotropic superconductors with $B_{c2}^{c} \ll B_P \ll B_{c2}^{ab}$. However, we note that such an exotic behavior is absent in so many low-dimensional TMDs with even stronger Pauli paramagnetic spin-splitting effects [8,9], which weakens the persuasion of this interpretation. Other important factors should be considered to interpret our experiments. One important clue for exploring the physical origination is that such a rare behavior was also observed in restacked 1T'-MoS_2 (see Figure S5) prepared with the similar process [26] to that used in restacked TaS_2. This implies that the unique and common features of such restacked monolayered materials are key factors for our observations. One most conspicuous feature for such restacked monolayer materials is the noncentrosymmetric crystal structure as mentioned in the beginning of the Results section. It has been discussed a lot both theoretically and experimentally that the noncentrosymmetric crystal structure along with strong spin-orbit coupling (SOC), which also exists in the present compound with 5d metal, is very favorable to incur the spin-triplet component in the superconducting order parameter [27–33]. This may be one possible origin of our observations. One positive evidence for this scenario is that the restacked 1T'-MoS_2, which have a weaker SOC because of the lighter 4d Mo element, shows an inconspicuous enhancement of $B_{c2}(\theta)$ compared with restacked TaS_2.

One possible extrinsic origination to explain our results comes from the possible orientation mismatch or wrinkles of the monolayer TaS_2 sheets during the restacking process, which affects the c-axis orientation of the restacked samples. However, the fact that the out-plane upper critical field B_{c2}^c of the restacked sample is very close to bilayer sample [13] indicates that such an effect, if it exists, should be very small since B_{c2}^c is expected to be enhanced obviously by some degree of the mixture of B_{c2}^{ab} component.

Importantly, the enhancement of upper critical field and critical transition temperature discovered here will show great values in both fundamental physics and practical applications. As shown by the dashed and dotted lines in Figure 2c, the upper critical field decreases quickly with the the direction diverging from $\theta = 90^o$ in the ordinary 2D or anistropic-3D superconductors, like the high-T_c cuprates, which set a strict restriction for the application in high field [34]. People may need to array the superconductors with $B \parallel ab$-plane strictly when applying in the environment of high field. Such a reduction of B_{c2} with θ is postponed greatly in our data indicated by blue curve in Figure 2c, which clearly facilitates the applications in high field.

To summarize, we have measured the angular-resolved electrical resistance of the restacked TaS_2 nanosheets in the external magnetic field along different directions. It is found that the Pauli paramagnetic limit is broken through in the mixed state, placing the the present superconducting system in the environment suffering a strong Pauli paramagnetic spin-splitting effects. Clear enhancement of the upper critical field and the critical transition temperature is observed in inclined magnetic field. Our analysis indicates that the highly noncentrosymmetric crystal structure and the strong spin-orbit coupling are key factors of the mechanism of the unusual behaviors we observed.

Methods

Sample preparation. The restacked TaS_2 nanosheets were obtained by a chemical exfoliation method followed by the vacuum filtration [11,12]. Firstly 2H-TaS_2 powders were prepared by the solid-states reaction. Then the Li_xTaS_2 powders were synthesized by soaking as-prepared 2H-TaS_2 powders in n-butyl lithium solution. The as-prepared Li_xTaS_2 crystals were exfoliated in distilled water. The redox reaction occurs at this stage. The obtained colloidal solution is composed of TaS_2 monolayers and is rather stable. The restacked TaS_2 nanosheets were obtained from the vacuum filtration of the colloidal suspension.

Resistance measurements The electrical transport data were collected by the standard four-probe method with magnetic field rotating in the plane perpendicular to the electric current. θ denoted the included angle between external field B and the c-axis of the crystal. The applied electric current is 10 μA when carrying out the measurements.

1. Ohtomo, A. & Hwang, H. Y. A high-mobility electron gas at the $LaAlO_3/SrTiO_3$ heterointerface. *Nature* **427**, 423–426 (2004).

2. Reyren, N. *et al.* Superconducting interfaces between insulating oxides. *Science* **317**, 1196–1199 (2007).

3. Gozar, A. *et al.* High-temperature interface superconductivity between metallic and insulating copper oxides. *Nature* **455**, 782–785 (2008).

4. Wang, Q.-Y. *et al.* Interface-induced high-temperature superconductivity in single unit-cell fese films on $SrTiO_3$. *Chinese Physics Letters* **29**, 037402 (2012).

5. Saito, Y., Nojima, T. & Iwasa, Y. Highly crystalline 2D superconductors. *Nature Reviews Materials* **2**, 16094 (2016).

6. Abrikosov, A. A. *Fundamentals of Theory of Metals* (Elsevier, 1988).

7. Xi, X. *et al.* Ising pairing in superconducting $NbSe_2$ atomic layers. *Nature Physics* **12**, 139 (2016).

8. Saito, Y. *et al.* Superconductivity protected by spincvalley locking in ion-gated MoS_2. *Nature Physics* **12**, 139 (2016).

9. Lu, J. M. *et al.* Evidence for two-dimensional ising superconductivity in gated MoS_2. *Science* **350**, 1353 (2015).

10. Xing, Y. *et al.* Ising superconductivity and quantum phase transition in macro-size monolayer $NbSe_2$. *Nano Lett.* **17**, 6802 (2017).

11. Pan, J. *et al.* Enhanced superconductivity in restacked TaS_2 nanosheets. *Journal of the American Chemical Society* **139**, 4623–4626 (2017).

12. Guo, C. *et al.* High-quality single-layer nanosheets of MS_2 (M = Mo, Nb, Ta, Ti) directly exfoliated from AMS_2 (A = Li, Na, K) crystals. *J. Mater. Chem. C* **5**, 5977–5983 (2017).

13. Yang, Y. *et al.* Enhanced superconductivity and suppression of charge-density wave order in 2H-TaS_2 in the two-dimensional limit. *arXiv:* 1711.00079 (2017).

14. Woollam, J. A. & Somoano, R. B. Superconducting critical fields of alkali and alkaline-earth intercalates of MoS_2. *Phys. Rev. B* **13**, 3843–3853 (1976).

15. Ma, Y. *et al.* Strong anisotropy effect in an iron-based superconductor $CaFe_{0.882}Co_{0.118}AsF$. *Superconductor Science and Technology* **30**, 074003 (2017).

16. Werthamer, N. R., Helfand, E. & Hohenberg, P. C. Temperature and purity dependence of the superconducting critical field, H_{c2}. III. electron spin and spin-orbit effects. *Phys. Rev.* **147**, 295–302 (1966).

17. Clogston, A. M. Upper limit for the critical field in hard superconductors. *Phys. Rev. Lett.* **9**, 266–267 (1962).

18. Yuan, F. F. *et al.* Anisotropy of iron-platinum-arsenide $Ca_{10}(Pt_nAs_8)(Fe_{2-x}Pt_xAs_2)_5$ single crystals. *Applied Physics Letters* **107**, 012602 (2015).

19. Blatter, G., Feigel'man, M. V., Geshkenbein, V. B., Larkin, A. I. & Vinokur, V. M. Vortices in high-temperature superconductors. *Rev. Mod. Phys.* **66**, 1125–1388 (1994).

20. Harper, F. E. & Tinkham, M. The mixed state in superconducting thin films. *Phys. Rev.* **172**, 441–450 (1968).

21. Zhou, W. *et al.* Anomalous electron doping independent two-dimensional superconductivity. *New Journal of Physics* **19**, 073014 (2017).

22. Wu, J. *et al.* Anomalous independence of interface superconductivity from carrier density. *Nat. Mater.* **12**, 877–881 (2013).

23. Lebed, A. G. Cooper pairs with broken parity and spin-rotational symmetries in d-wave superconductors. *Phys. Rev. Lett.* **96**, 037002 (2006).

24. Lebed, A. G. Type-IV superconductivity: Can superconductivity be more exotic than unconventional? *Journal of Low Temperature Physics* **142**, 173–178 (2006).

25. Dutta, O. & Lebed, A. G. Cooper pairs with broken time-reversal, parity, and spin-rotational symmetries in singlet type-II superconductors. *Phys. Rev. B* **78**, 224504 (2008).

26. Fang, Y. *et al.* Structure re-determination and superconductivity observation of bulk 1T MoS_2. *Angewandte Chemie International Edition* DOI: 10.1002/anie.201710512 (in press) (2017).

27. Gor'kov, L. P. & Rashba, E. I. Superconducting 2D system with lifted spin degeneracy: Mixed singlet-triplet state. *Phys. Rev. Lett.* **87**, 037004 (2001).

28. Frigeri, P. A., Agterberg, D. F., Koga, A. & Sigrist, M. Superconductivity without inversion symmetry: MnSi versus $CePt_3Si$. *Phys. Rev. Lett.* **92**, 097001 (2004).

29. Samokhin, K. V. Paramagnetic properties of noncentrosymmetric superconductors: Application to $CePt_3Si$. *Phys. Rev. Lett.* **94**, 027004 (2005).

30. Frigeri, P. A., Agterberg, D. F. & Sigrist, M. Spin susceptibility in superconductors without inversion symmetry. *New Journal of Physics* **6**, 115 (2004).

31. Yuan, H. Q. *et al.* S-wave spin-triplet order in superconductors without inversion symmetry: Li_2Pd_3B and Li_2Pt_3B. *Phys. Rev. Lett.* **97**, 017006 (2006).

32. Nishiyama, M., Inada, Y. & Zheng, G.-q. Spin triplet superconducting state due to broken inversion symmetry in Li_2Pt_3B. *Phys. Rev. Lett.* **98**, 047002 (2007).

33. Yogi, M. *et al.* Evidence for novel pairing state in noncentrosymmetric superconductor $CePt_3Si$: ^{29}Si-NMR knight shift study. *Journal of the Physical Society of Japan* **75**, 013709 (2006).

34. Cai, C., Holzapfel, B., Hänisch, J. & Schultz, L. Direct evidence for tailorable flux-pinning force and its anisotropy in $RBa_2Cu_3O_{7-\delta}$ multilayers. *Phys. Rev. B* **70**, 212501 (2004).

Acknowledgments

This work is supported by the National Natural Science Foundation of China (No. 11204338), the "Strategic Priority Research Program (B)" of the Chinese Academy of Sciences (No. XDB04040300, and XDB04030000) and Youth Innovation Promotion Association of the Chinese Academy of Sciences (No. 2015187).

Author contributions

G.M. and F.Q.H. designed the experiments. Y.H.M. performed the measurements. J.P. and C.G.G. synthesized the samples. G.M. analysed the data. Y.H.M., J.P., C.G.G. X.Z., L.L.W., T.H., G.M., F.Q.H., and X.M.X. discussed the results. G.M. and F.Q.H. wrote the paper. X.M.X. supervised the work.

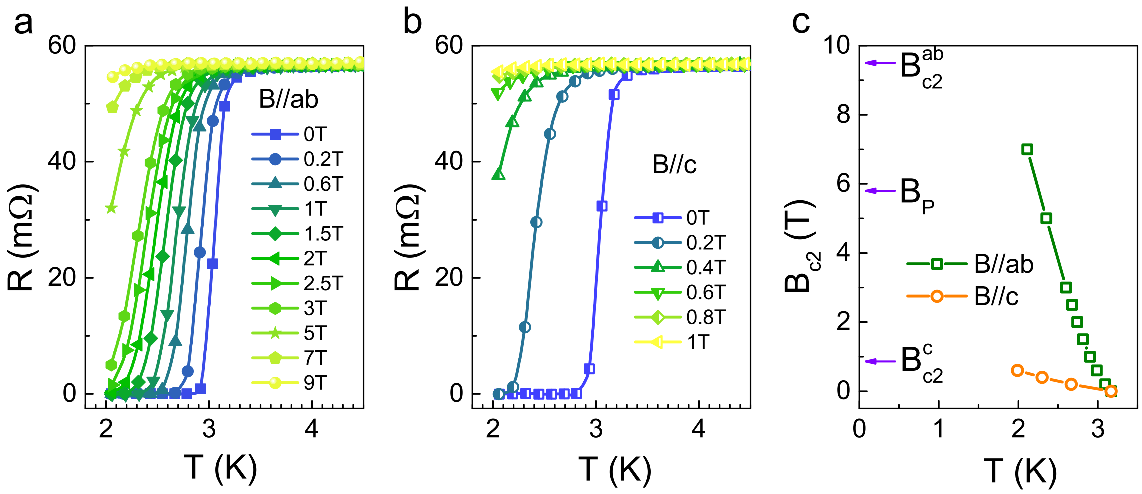

Figure 1 Temperature dependence of the resistive transitions under magnetic field for the sample #1. (a) $B \parallel ab$. (b) $B \parallel c$. (c) $B_{c2} - T$ phase diagram obtained using the criterion 90%R_n. The three characteristic fields B_{c2}^{ab}, B_{c2}^{c} and B_P are indicated by the arrows in this figure.

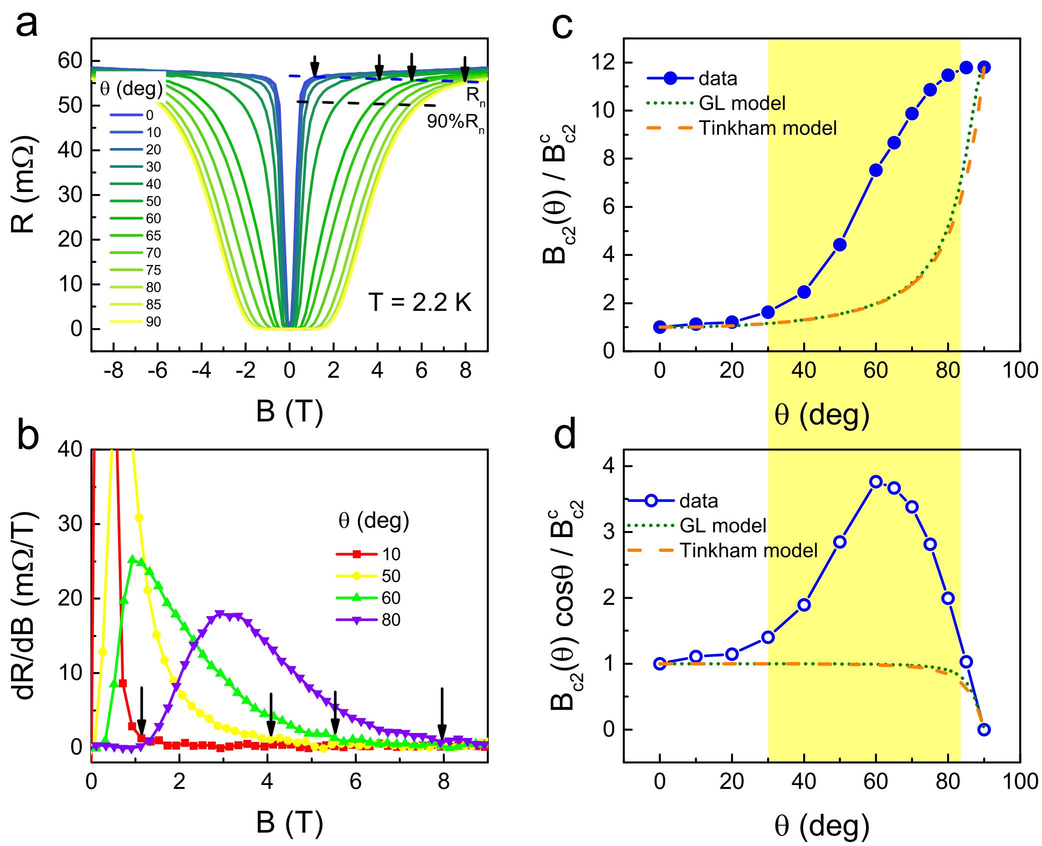

Figure 2 The measurements of the upper critical field along different directions $B_{c2}(\theta)$ for sample #1. (a) Field dependence of resistance with the external field rotating from $B \parallel c$ ($\theta = 0^o$) to $B \parallel ab$ ($\theta = 90^o$) at a fixed temperature $T = 2.2$ K. (b) Differential of the $R - B$ curves in (a), based on which the onset superconducting transition points are determined indicated by the black arrows. (c) Angular dependence of the upper critical field $B_{c2}(\theta)$ normalized by B_{c2}^c. (d) Field dependence of perpendicular component of the upper critical field $B_{c2}(\theta)cos\theta$ normalized by B_{c2}^c. In (c) and (d), the theoretical curves based on the GL model and Tinkham model are shown in comparison with the experimental data.

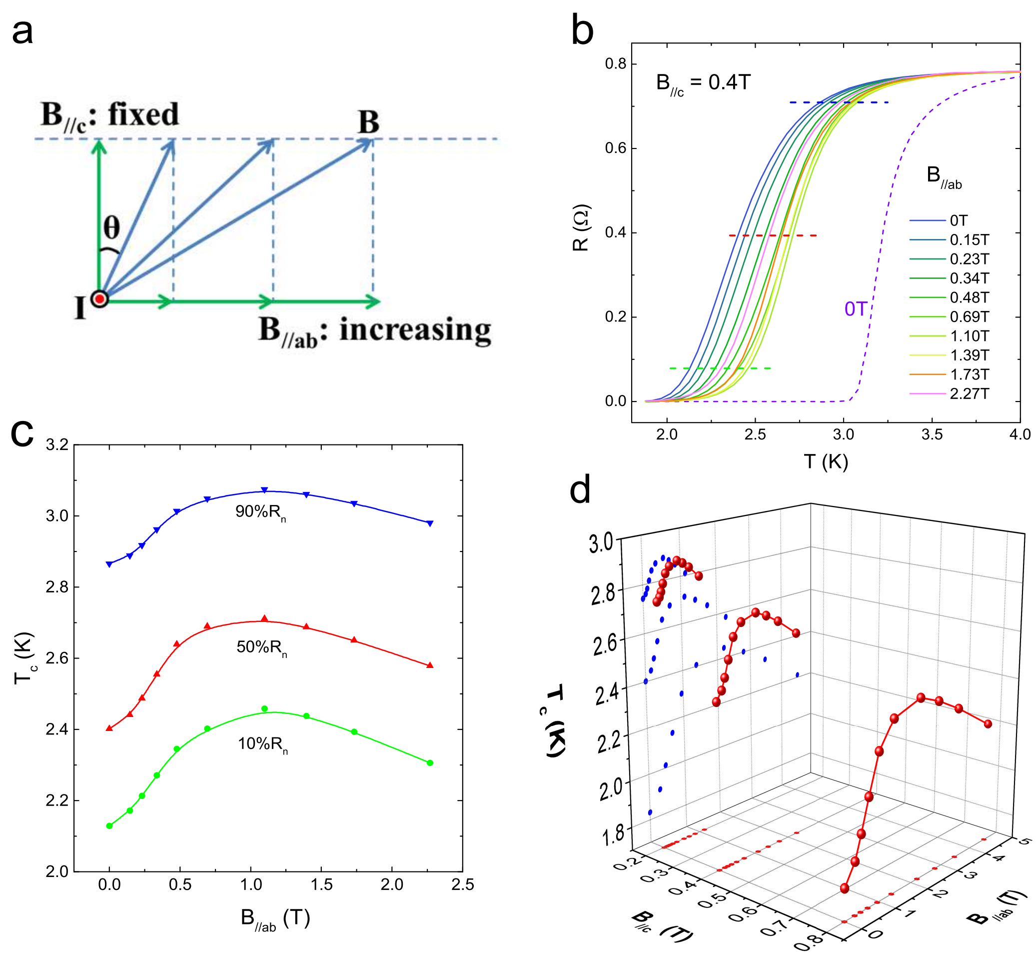

Figure 3 Electrical resistance data and the critical transition temperature in the inclined field with $B_{\parallel c}$ fixed and $B_{\parallel ab}$ increasing for sample #2. (a) Sketch map of the field configuration for the measurements. (b) $R-T$ curves with $B_{\parallel c}$ = 0.4 T and $B_{\parallel ab}$ increasing. (c) $B_{\parallel ab}$ dependence of T_c determined from the data in (b) by three criterions 10%R_n, 50%R_n and 90%R_n. (d) $B_{\parallel ab}$ dependence of T_c by the criterion 50%R_n under three fixed $B_{\parallel c}$ = 0.2 T, 0.4 T and 0.8 T.

Table 1: Summary of the upper critical fields (B_{c2}^{ab} and B_{c2}^{c}) and the paramagnetic limiting field (B_P) of the sample #1.

T_c	$dB_{c2}^{ab}(T)/dT\|_{T_c}$	$dB_{c2}^{c}(T)/dT\|_{T_c}$	B_{c2}^{ab}	B_{c2}^{c}	B_P
3.17 K	-4.34 T/K	-0.39 T/K	9.5 T	0.86 T	5.8 T